Original

Burkhardt, I.; Ventzke, V.; Riekehr, S.; Kashaev, N.; Enz, J.:

Development of an optimised shielding strategy for laser beam welding of Ti6Al2Sn4Zr2Mo

In: Materials Science Forum, THERMEC 2018 (2018) Trans Tech Publications

DOI: 10.4028/www.scientific.net/MSF.941.1404

Materials Science Forum *Online: 2018-12-26*
ISSN: 1662-9752, Vol. 941, pp 1404-1410
doi:10.4028/www.scientific.net/MSF.941.1404

Development of an Optimised Shielding Strategy for Laser Beam Welding of Ti6Al2Sn4Zr2Mo

Irmela Burkhardt[1,a*], Volker Ventzke[1,b], Stefan Riekehr[1,c], Nikolai Kashaev[1,d], Josephin Enz[1,e]

[1]Helmholtz-Zentrum Geesthacht, Institute of Materials Research, Materials Mechanics, Joining and Assessment, Max-Planck-Straße 1, 21502 Geesthacht, Germany

[a]irmela.burkhardt@hzg.de, [b]volker.ventzke@hzg.de, [c]stefan.riekehr@hzg.de, [d]nikolai.kashaev@hzg.de, [e]josephin.enz@hzg.de

Keywords: laser beam welding; Ti alloy; shielding gas; fibre laser; laser beam attenuation.

Abstract. Ti6Al2Sn4Zr2Mo exhibits improved oxidation and creep properties compared to Ti6Al4V. Laser beam welding (LBW) is an approved process to receive narrow weld seams at high welding speeds with low heat input. Almost distortion free complex shaped structures can be joined with optimal parameters. For the optimisation of the LBW process the most relevant parameters are the welding speed, the laser input power and the gas shielding strategy. Using a fibre laser, the laser radiation is attenuated by a welding plume the so-called metal-vapour cloud (MVC). The MVC has a large influence on the laser input power. Therefore, an approach for reducing the MVC by optimising the shielding strategy using an additional gas flow in opposite welding direction is examined. Utilizing high-speed camera records, the effectiveness of the approach is assessed. Welded samples are evaluated by visual and radiographic inspection, metallographic assessment as well as microhardness measurements with regard to weld seam geometry, defects, microstructure and local mechanical properties. The obtained results are correlated to the used laser welding parameters.

Introduction

The light-metal titanium is utilized in a large application field from aerospace to medical industry. Ti6Al2Sn4Zr2Mo (Ti6242) is a near-α high temperature alloy. The higher creep resistance [1] and lower oxidation kinetics [2] compared to Ti6Al4V (Ti64) are beneficial for high temperature applications in aircrafts. Since Ti alloys exhibit high affinity to air constituents [3], shielding gas is needed during welding to protect the weld pool against oxidation. For complex structures, especially in the aircraft industry, high-integrity is demanded and can be implemented by the use of fusion welding methods like laser beam welding. Furthermore, laser welding offers low process times, high flexibility of the welded geometry and a small heat-affected zone (HAZ) [4,5]. Fibre lasers are advantageous in comparison to CO_2 lasers because the absorption of laser radiation by the plasma plume can be neglected [6]. Nevertheless, for fibre lasers another shielding effect occurs. A so-called metal vapour cloud (MVC), consisting of small particles, is formed. These particles generally absorb and scatter a portion of the laser radiation. Therefore, the laser radiation is attenuated above the deep penetration channel and consequently the laser energy is only partly coupled into the material [7]. A cross-jet in welding direction showed to be insufficient for removing the MVC [6]. The heat-input itself and thus the line energy (LE) influences the resulting weld seam shape. Using low LE results in a V-shaped weld seam [8], which is associated with the closed keyhole mode [9]. In contrast, a high LE leads to an X-shaped weld seam [8] and an open keyhole mode. A closed keyhole mode has a higher melting efficiency; however through an open keyhole entrapped gases can escape through the top and the bottom [9]. The plume dynamic is linked to the keyhole oscillation and therefore to the process stability. Violent evaporations on the keyhole wall lead to a swing of the plume and gas is entrapped [10]. The possibility for process-induced porosity is high for larger weld pools, since a more complex fluid system with recirculation at the bottom occurs. Consequently, an increase in welding speed, and thus a decrease in energy

density, is favourable for reducing the weld pool size and the probability for pore formation [11]. Furthermore, during high cycle fatigue tests with Ti-6Al-4V butt joints all fractures occurred from internal pores and clusters of pores [12]. Two grain structures were typically reported in the fusion zone (FZ). In the middle of the FZ, straight axial columnar grains with a growing direction in welding direction and curved columnar grains growing from the FZ boundary occur [13]. During transvers tensile tests for aluminium, failure occurred in regions with axial columnar grains [14]. Furthermore, axial grains are susceptible to centreline solidification cracks [15]. The width and height of the axial columnar grains can be reduced by increasing the welding speed [13].

In this study the influence of a cross-jet in opposite welding direction, in order to reduce the MVC and therefore stabilizing the welding process, is investigated. Furthermore, the effect of the cross-jet on the microstructure, weld seam geometry and the local mechanical properties is analyzed.

Experimental Procedure

As a welding material 2 mm thick Ti6242 is used. The weld coupons are 50 mm x 25 mm x 2mm large. Prior to welding the welding edge was milled and cleaned with methylated aceton. For welding an 8 kW fiber laser (IPG YLS-8000) equipped with a 300 mm focusing optic, a 300 mm fibre and a focus diameter of 746 µm was utilized. The experimental set-up (s. Figure 1) was mounted in a CNC-machine center (IXION ULM). The weld coupons were clamped in a gas shielding box, flooded with argon (15 l/min) and the laser focus position was placed on the sheet surface (0 mm). The cross-jet nozzle was positioned 1 mm away from the laser beam in opposite welding direction and 15 mm above the weld coupon. A high-speed camera monitored the welding process.

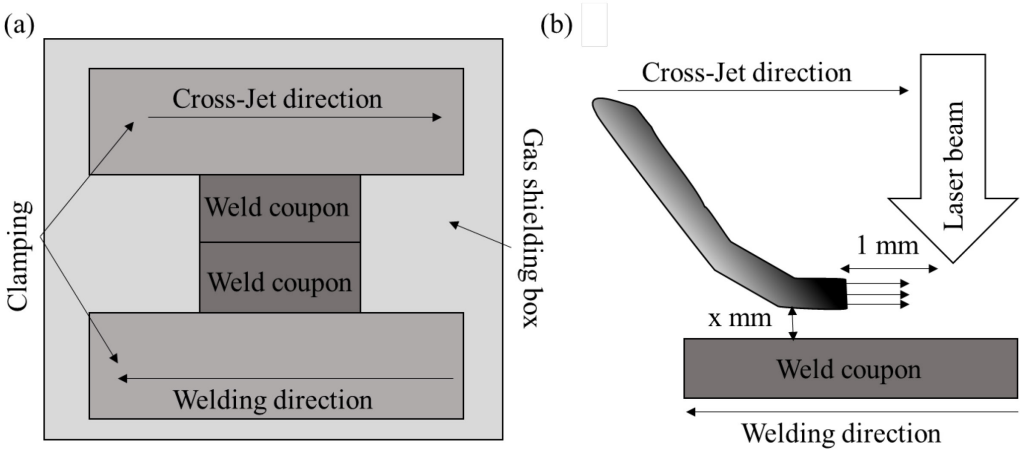

Figure 1: (a) Top and (b) side view of the schematic experimental set-up.

For welding experiments without cross-jet, laser powers (P) between 1.75 kW and 8 kW and welding speeds (v) between 0.7 mm to 5 m/min were utilized. Using a cross-jet flow rate between 10 l/min and 20 l/min, P was set to 2 kW or 2.5 kW with v between 2 m/min and 5 m/min.

Welded samples were visually and radiographically inspected. The resolution limit for radiography was 50 µm. Cross-section were taken from the middle of the weld seam. After grinding, polishing and etching with Kroll's solution, cross-sections were analyzed by optical microscopy. The weld seam width corresponds to FZ width. Vickers microhardness measurements were performed in the middle of the weld seam with a load of 300 g, a intrude velocity of 0.1 mm/min and a dwelling time of 15 s. The distance between the indentations was 0.16 µm

Results and Discussion

Using a cross-jet in opposite welding direction, the MVC could be successfully reduced (s. Figure 2) For 2.5 kW and 3 m/min the threshold value seems to be 15 l/min (s. Figure 2 (c)). The difference in MVC between 15 l/min and 20 l/min is negligible (s. Figure 2 (c), (d)). Furthermore, the high-speed records showed less swinging, when the cross-jet was used. Thus, the cross-jet stabilizes the welding process. Moreover, the visual inspection showed, that more spatter occurs with a cross-jet flow rate of 20 l/min compared to 15 l/min. Consequently, for 2 kW the maximum cross-jet flow rate was 15 l/min.

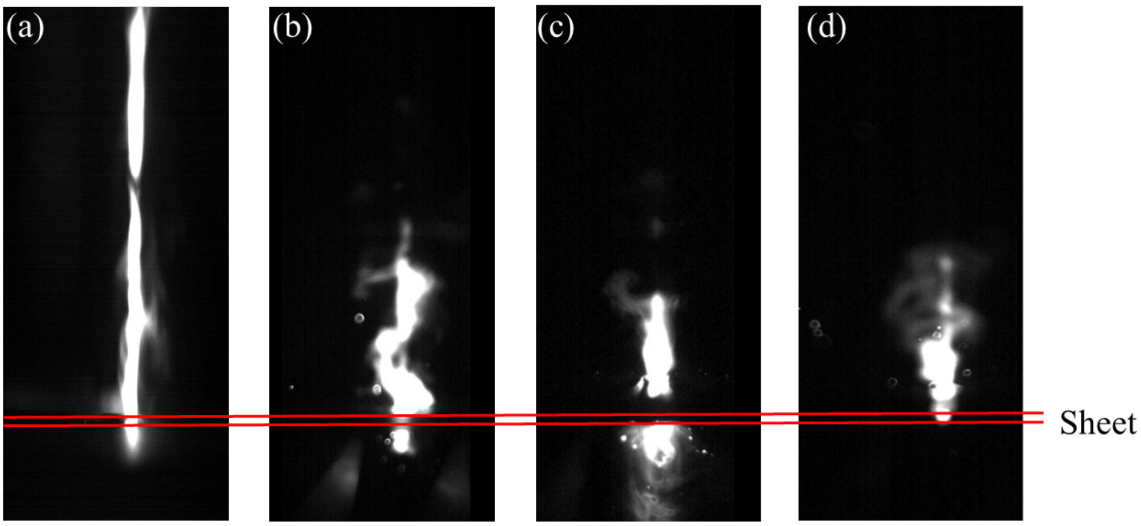

Figure 2: High-speed camera images. Parameter set 2.5 kW, 3 m/min. Cross-jet gas flow rate: (a) 0 l/min. (b) 10 l/min. (c) 15 l/min. (d) 20 l/min.

Radiography analysis revealed line porosity for 2 kW and 2 m/min. Using a cross-jet of 10 l/min and a higher v, full penetration was achieved and the line porosity was removed. This is consistent with the high-speed camera records, showing that the cross-jet reduces the swinging of the MVC and thus stabilization of the welding process. The other welds were free of line porosity (s. Figure 3, Figure 4). The average pore size utilizing a cross-jet was between 0.15 mm and 0.3 mm.
To achieve an open keyhole mode and thus a X-shaped weld seam without a cross-jet, small v are necessary for low P (s. Figure 3 (a)). Since the FZ is larger, the weld pool was large and the possibility for process-induced porosity is high [11]. To achieve smaller welds seams with a tendency to form an I-shape, an increase in v and higher P are mandatory (s. Figure 3 (b), (c)).

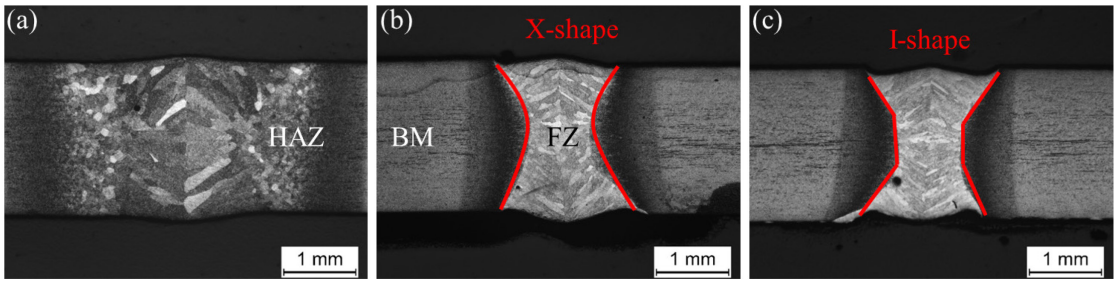

Figure 3: Cross-Section of (a) 1.75 kW, 0.7 m/min, (b) 4.5 kW, 4 m/min and (c) 8 kW, 5 m/min. HAZ: Heat-affected zone. FZ: Fusion zone. BM: Base material.

Increasing P from 2 kW to 2.5 kW with a v of 2 m/min, results in a change of the weld seam shape form Y to X (s. Figure 4). Increasing v from 2 m/min to 3 m/min with 2.5 kW, the shape changes back to Y, which is consistent with the observations in literature [8]. By reducing the MVC with a cross-jet of 10 l/min, P=2.5 kW and v=3 m/min, an X-shaped weld seam is achieved. Therefore, the effective LE coupled into the material is increased by this reduction of the MVC. Furthermore, using a cross-jet of 15 l/min or 20 l/min, full penetration with v up to 5 m/min could be realized for 2 kW and 2.5 kW. Consistent with the high-speed camera results for 2.5 kW, no

considerable weld seam shape differences are observed for high cross-jet flow rates (s. Figure 4). Increasing v up to 5 m/min, utilizing 2.5 kW and 15 l/min for the cross-jet, the formation of an I-shaped weld seam is most likely. Without a cross-jet, for example 8 kW and 5 m/min are necessary for an I-shaped weld seam (s. Figure 3 (c)). A narrow I-shaped weld seam is beneficial, since the weld pool is smaller and the microstructure in the FZ finer. A finer microstructure has a higher crack initiation resistance than a coarser microstructure [16] and an I-shaped weld seam would be advantageous for the stress distribution along the fusion line. Furthermore, a small weld pool reduces the possibility for process-induced pores [11], which are the cause of fracture in high cycle fatigue tests [12].

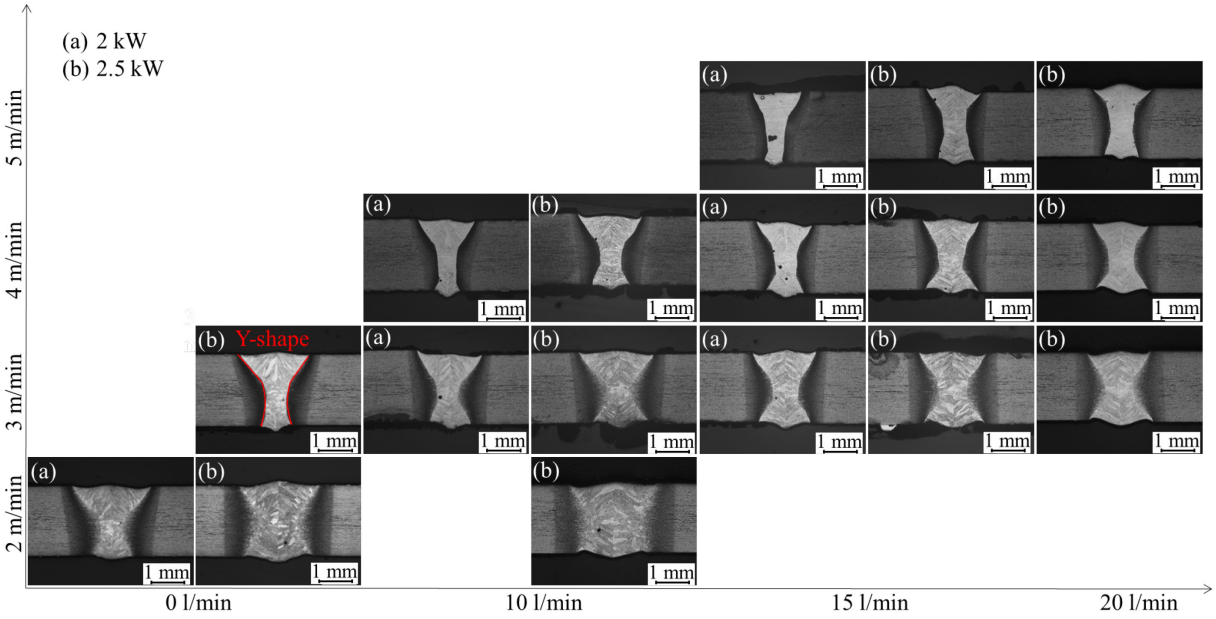

Figure 4: Cross-sections of (a) 2 kW and (b) 2.5 kW with different welding speeds and cross-jet flow rates.

With increasing v the average weld seam width for 2 kW and 2.5 kW decreases (s. Figure 5). Although the use of a cross-jet changes the weld seam shape, it has no significant influence on the average weld seam width. Similar to the average weld seam width, the average HAZ width decreases with v and the cross-jet influence is negligible.

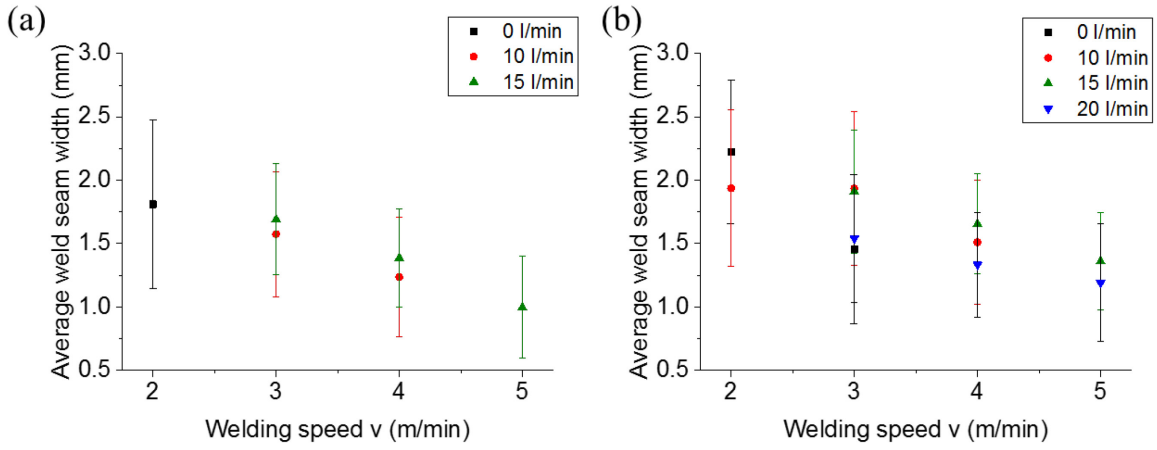

Figure 5: Average weld seam width of (a) 2 kW and (b) 2.5 kW for different welding speeds and cross-jet flow rates.

Weld seams, laser beam welded with and without cross-jet, show a microhardness increase from the base material (BM) to the FZ (s. Figure 6) due to formation of martensitic microstructure in FZ. Expect of a minor microhardness decrease in the FZ for 1.75 kW and 0.7 m/min, the microhardness profiles without cross-jet is independent of P and v (s. Figure 6(a)). Using a cross-jet in opposite welding direction leads to similar microhardness profiles (s. Figure 6). Due to the use of a cross-jet,

a higher cooling rate for the weld seam solidification could occur, resulting in a higher microhardness. Nevertheless, the microhardness profiles using different cross-jet flow rates, 2.5 kW and 3 m/min have similar profiles and values. Consequently, the cross-jet do not show any significant effect on the microhardness. Possibly, the effective higher energy input by utilizing the cross-jet as described earlier compensates this cooling effect of the cross-jet.

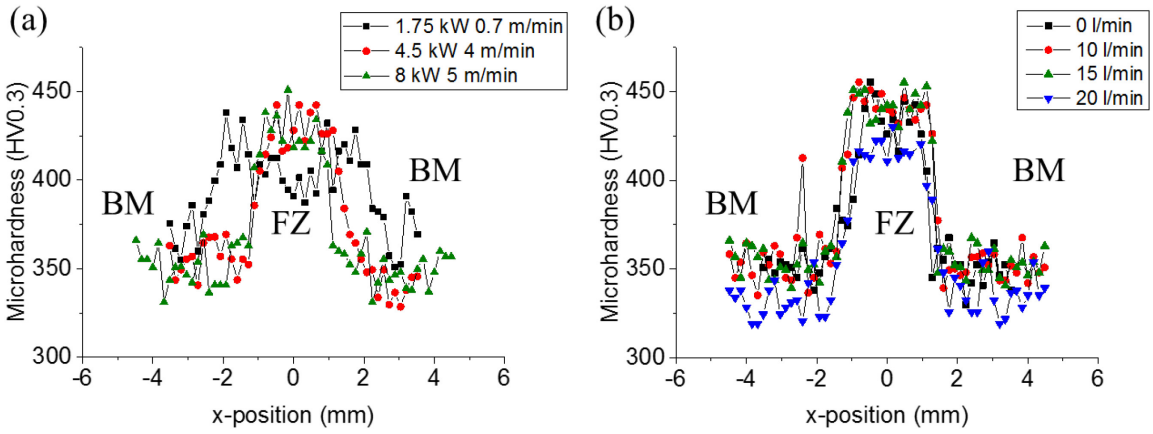

Figure 6: Microhardness profile (a) without cross-jet for different parameter sets and (b) for different cross-jet flow rates using 2.5 kW and 3 m/min.

Analyzing the microhardness in the FZ (s. Figure 7), it turns out that the microhardness values using 2 kW, different v and different cross-jet flow rates are within the standard deviation (s. Figure 7 (a)). The deviation for 2.5 kW are larger than for 2 kW (s. Figure 7). This could be due to measurement deviations or minor microstructure differences. Nevertheless, the microhardness difference is smaller than 10 % and hence not significant.

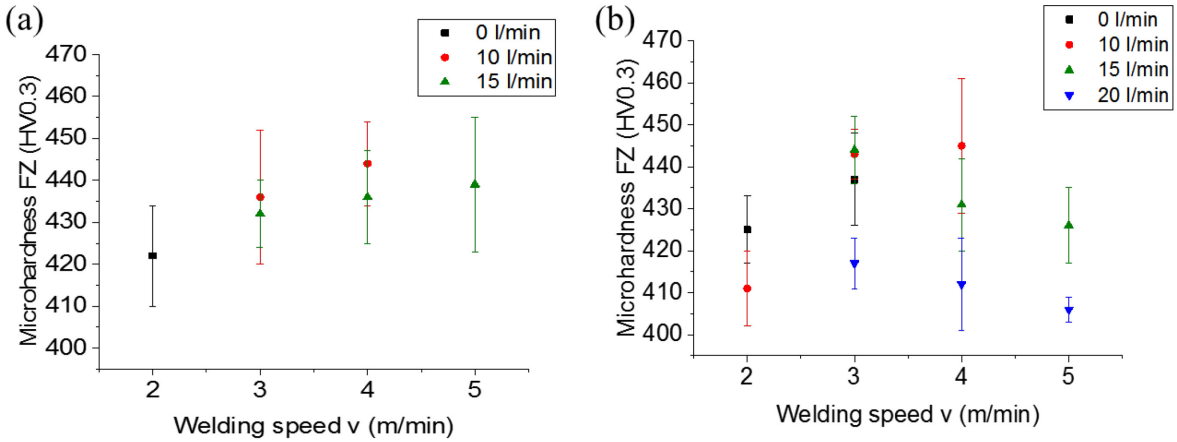

Figure 7: Average microhardness in the fusion zone (FZ) of (a) 2 kW and (b) 2.5 kW.

Summary

The metal vapour cloud was successfully reduced using a cross-jet in opposite welding direction. The minimal cross-jet flow rate for a laser power of 2.5 kW was 15 l/min. High-speed camera records showed a reduced height and less swinging of the plume during the use of a cross-jet, indicating a stabilization of the welding process. As a result, line porosity could also be removed. With increased laser power, welding speed and cross-jet flow rate the amount of spatter increased. In combination with an increasing welding speed, the reduced metal vapour cloud resulted in a change of weld seam shape from Y- via X- to an I-shape. Because of the higher heat input coupled into the material, higher welding speeds could be used. Without a cross-jet the formation of an I-shaped weld seam was here only achieved with the parameter set 8 kW and 5 m/min. Using a cross-jet, welding speeds up to 5 m/min with 2 kW or 2.5 kW still lead to full penetration welds. Furthermore, using a cross-jet flow rate of 15 l/min or 20 l/min, I-shaped weld seams were

accomplished. Thus, a cross-jet is beneficial for achieving an I-shaped weld seam, if low laser powers and high welding speeds are applied. With increasing welding speed the average weld seam and average heat-affected zone width decreases. Moreover, a finer microstructure was achieved with higher welding speeds. Vickers microhardness measurements revealed no considerable influence of the laser power, welding speed and cross-jet flow rate on the mircorhardness profile and average microhardness in the fusion zone.

Acknowlegment

The work was carried out under the auspices of the TiB-Air project (project number: 20W1522C), which was funded by the German Federal Ministry of Economics and Technology (BMWi) under the LuFo V-2 program. The authors would like to thank the BMWi for the financial support as well as René Dinse, Falk Dorn and Peter Haack for their valuable technical support.

References

[1] E. G. Welsch, R.Boyer, Materials Properties Handbook: Titanium Alloys, ASM International, Materials Park, 1998.

[2] R. Gaddam, B. Sefer, R. Pederson, M.L. Antti, Oxidation and alpha-case formation in Ti-6Al-2Sn-4Zr-2Mo alloy, Mater. Charact. 99 (2015) 166–174. doi:10.1016/j.matchar.2014.11.023.

[3] M. Peters, C. Leyens, Titan und Titanlegierungen, WILEY-VCH, Weinheim, 2002.

[4] C. Dawes, Laser welding, a practical guide, Abington Publishing, Cambridge, 1992.

[5] E. Akman, A. Demir, T. Canel, T. Sinmazçelik, Laser welding of Ti6Al4V titanium alloys, J. Mater. Process. Technol. 209 (2009) 3705–3713. doi:10.1016/j.jmatprotec.2008.08.026.

[6] S.A. Uspenskiy, V.N. Petrovskiy, D.P. Bykovskiy, V.D. Mironov, N.M. Prokopova, E. V Tret'yakov, Spectral diagnostics of a vapor-plasma plume produced during welding titanium with a high-power ytterbium fiber laser, J. Phys. Conf. Ser. 594 (2015) 12033. doi:10.1088/1742-6596/594/1/012033.

[7] P.Y. Shcheglov, S.A. Uspenskiy, A. V Gumenyuk, V.N. Petrovskiy, M. Rethmeier, V.M. Yermachenko, Plume attenuation of laser radiation during high power fiber laser welding, Laser Phys. Lett. 8 (2011) 475–480. doi:DOI 10.1002/lapl.201110010.

[8] G. Casalino, M. Mortello, S.L. Campanelli, Ytterbium fiber laser welding of Ti6Al4V alloy, J. Manuf. Process. 20 (2015) 250–256. doi:10.1016/j.jmapro.2015.07.003.

[9] M.Y. Krasnoperov, R.R.G.M. Pieters, I.M. Richardson, Weld pool geometry during keyhole laser welding of thin steel sheets, Sci. Technol. Weld. Join. 9 (2004) 501–506. doi:10.1179/136217104225021733.

[10] S. Pang, X. Chen, X. Shao, S. Gong, J. Xiao, Dynamics of vapor plume in transient keyhole during laser welding of stainless steel: Local evaporation, plume swing and gas entrapment into porosity, Opt. Lasers Eng. 82 (2016) 28–40. doi:10.1016/j.optlaseng.2016.01.019.

[11] C. Panwisawas, B. Perumal, R.M. Ward, N. Turner, R.P. Turner, J.W. Brooks, H.C. Basoalto, Keyhole formation and thermal fluid flow-induced porosity during laser fusion welding in titanium alloys: Experimental and modelling, Acta Mater. 126 (2017) 251–263. doi:10.1016/j.actamat.2016.12.062.

[12] F. Fomin, N. Kashaev, Influence of Porosity on the High Cycle Fatigue Behaviour of Laser Beam Welded Ti-6Al-4V Butt Joints, Procedia Struct. Integr. 7 (2017) 415–422.

[13] H.L. Wei, J.W. Elmer, T. DebRoy, Crystal growth during keyhole mode laser welding, Acta Mater. 133 (2017) 10–20. doi:10.1016/j.actamat.2017.04.074.

[14] S.R.K. Rao, G.M. Reddy, M. Kamaraj, K.P. Rao, Grain refinement through arc manipulation techniques in Al-Cu alloy GTA welds, Mater. Sci. Eng. A. 404 (2005) 227–234.

[15] S. Kou, Welding Metallurgy, second ed., Hoboken, NJ, 2003.

[16] O. Jin, S. Mall, Effects of microstructure on short crack growth behavior of Ti-6Al-2Sn-4Zr-2Mo-0.1Si alloy, Mater. Sci. Eng. A. 359 (2003) 356–367. doi:10.1016/S0921-5093(03)00377-0.